Soft Matter

Accepted Manuscript

ROYAL SOCIETY OF CHEMISTRY

www.rsc.org/softmatter

Cite this: DOI: 10.1039/c0xx00000x

www.rsc.org/xxxxxx

PAPER

Elucidating and tuning the strain-induced non-linear behavior of polymer nanocomposites: a detailed molecular dynamics simulation study

Jianxiang Shen,[a] Jun Liu,[a] Yangyang Gao,[a] Xiaolin Li[a] and Liqun Zhang*[a,b,c]

Received (in XXX, XXX) Xth XXXXXXXXX 20XX, Accepted Xth XXXXXXXXX 20XX
DOI: 10.1039/b000000x

By setting up a coarse-grained model of polymer nanocomposites, we monitored the change in elastic modulus as a function of the strain, derived from the stress-strain behavior by performing the uniaxial tension and simple shear of two typical spatial distribution states(aggregation vs. dispersion) of nanoparticles(NPs). In both cases, we observed that the elastic modulus decreases non-linearly with the increase of strain and reaches a low plateau at large strains. This phenomenon is similar to the so-called "Payne effect" for elastomer nanocomposites. Particularly, the modulus of the aggregation case is more sensitive to the imposed strain. By examining the structural parameters such as the number of neighboring NPs, coordination number of NPs, root-mean-squared average force exerted on the NPs, local strain, chain conformations(bridge, dangle, loop, interface bead and connection bead), and the total interaction energy of NP-polymer and NP-NP, we inferred that the underlying mechanism of the aggregation case is the breakup of the NP network or clusters formed through direct contact, while for the dispersion case the non-linear behavior is attributed to the destruction of the NP network or clusters formed through the bridging of adsorbed polymer segments among the NPs. The former physical network is influenced by NP-NP interaction and NP volume fraction, while the latter is influenced by NP-polymer interaction and NP volume fraction. Lastly we found that for the dispersion case, further increasing the inter-particle distance or grafting NPs with polymer chains can effectively reduce the non-linear behavior due to the decrease of the physical network density. In general, this simulation work for the first time establishes the correlation between the micro-structural evolution and the strain-induced non-linear behavior of polymer nanocomposites, and sheds some light on how to reduce the "Payne effect".

1. Introduction

The reinforcement of elastomers which are well-known for their unique ability to withstand large deformations and the reversibility is of great interest and importance.[1-7] The strength and modulus of particulate-filled polymer composites, as an important part of reinforcement, are crucially influenced by the size, shape, content, and spatial distribution of the inclusions as well as the interfacial compatibility between the polymer matrix and the inclusions.[8-16] However, as these influencing factors are closely correlated, few consistent conclusions on the reinforcement mechanism have been reached. Actually, the non-linear behaviors under deformation conditions play an important role in the understanding of reinforcement mechanism of particulate-filled elastomeric materials.[7, 17-19] The amplitude-dependence of the dynamic viscoelastic properties such as the storage and loss modulus is often referred as the Payne effect[20]. And the viscoelastic behavior with hysteresis under cyclic uniaxial tension and recovery processes is generally termed as the Mullins effect which is also pointed to the stress softening.[21]

Some valuable information about the reinforcement mechanism can be obtained by studying the non-linear behaviors of polymer nanocomposites. For example, one contribution to the reinforcement comes from the polymer network related to the crosslink density and the chemical structure of polymer chains. Another contribution results from the hydrodynamic effect or the strain amplification, since the introduced rigid filler in the soft rubbery matrix cannot be deformed. Therefore, the intrinsic strain of the polymer matrix is much greater than the external strain, resulting in a strain-independent modulus.[22]

Moreover, the contribution from the effect of "in-rubber structure" is studied.[11, 12, 23-25] The primary particles assemble to form three-dimensional branched clusters called aggregates. These aggregates may be linked to form loose agglomerates by

[a]*Key Laboratory of Beijing City on Preparation and Processing of Novel Polymer Materials, Beijing University of Chemical Technology;*
[b]*Beijing Engineering Research Center of Advanced Elastomers, Beijing University of Chemical Technology;*
[c]*State Key Laboratory of Organic and Inorganic Composite Materials, Beijing University of Chemical Technology, Beijing 100029, P. R. China;*
E-mail:zhanglq@mail.buct.edu.cn
E-mail:zhanglq@mail.buct.edu.cn

van der Waals interactions. Therefore, the occluded rubber in the voids between the aggregates and agglomerates is shielded from deformation and thus the effective filler content is increased, leading to a strain-independent contribution to the modulus. For example, by the self-consistent approach, Omnès[10] proposed a morphological pattern for the microstructure as a combination of the occluded rubber, the bound rubber and a percolating network to estimate the elastic properties.

The non-linear behaviors at small amplitudes are also considered to be caused by the breakdown of the inter-aggregate association or the network structure of the fillers.[6, 26] The concept of filler network breakdown seems to be valid in interpreting the strain-dependence of dynamic mechanical properties.[13, 27-30] For example, Lame[31] observed the local deformation and the fracture of the filler networks under deformations by in-situ AFM scanning. J. Fröhlich et al.[32] investigated the strength of filler network and the filler-polymer interaction by Rubber-Process-Analyzer (RPA), and regarded these two factors to be responsible for the low strain modulus. Furthermore, based on the filler network, Stockelhuber et al.[33] proposed a layered fiber model to interpret the non-linear characteristics of the elastic and the viscous modulus of elastomer materials at high strain amplitudes.

Besides, the long-range filler network (or "polymer-mediated filler network") was reported to provide efficient reinforcement to elastomer materials.[1, 14, 34-40] In the polymer-mediated filler network, fillers are connect with each other through polymer chain segments. For example, the molecular arrangements such as the "loop", "dangle" and "bridge" structures in polymers filled with randomly distributed NPs under quiescent condition were analyzed by Vacatello[41, 42] by Monte Carlo simulations. And Sternstein and Zhu[43, 44] believed that the polymer structures of "chain loops" trapped on the filler surface as well as the entanglements characteristics of polymer chains and the molecular weight of the polymer matrix are the primary factors influencing the non-linear viscoelasticity of elastomer materials. Moreover, by investigating the non-linear viscoelastic behavior of silica-filled un-crosslinked polybutadiene, Zhu and his coworkers[14] suggested that the filler association through chain adsorption and bridging enhances reinforcement.

Particularly, the glassy polymer layers are reported to form in the vicinity of fillers.[45, 46] For instance, Berriot and Montes[47-50] along with their co-workers observed a glass transition temperature gradient in the vicinity of the particles. They believed that it is the glassy layer that leads to the non-linear viscoelastic behavior in reinforced elastomers. Moreover, Merabia et al.[51] described a microscopic model for the reinforcement of filled elastomers. They pointed out that strong reinforcement can be achieved when the glassy layers between fillers overlap, and it is particularly strong when the corresponding cluster fillers with glassy layers percolate. They also showed that the dynamics of yield and rebirth of glassy bridges can account for the non-linear behaviors. In addition, other factors such as the entanglement of polymer chains[52], the chain scissions[53], and the chain segment orientation[54] are also mentioned to contribute to the non-linear behaviors of elastomer materials.

Actually, from a microscopic point of view, the reinforcement of elastomeric materials involves various length and time scales[51, 55, 56]. For example, on the nanoscopic scale, the primary particles of carbon black fillers are more or less spherical particles of typical diameter 10 nm. The primary particles are assembled into fractal aggregates of typical diameter 100 nm. Therefore, the geometric shapes and the physical and chemical interactions between the polymer and primary fillers determine the reinforcement. On the mesoscopic scale, the aggregates and the filler network play an important role in the reinforcement. Since it is difficult to directly characterize the complicated micro-structure of elastomer nanocomposites through experimental tools, computer modeling and simulation have been used for such purpose.[15, 57, 58] For instance, Mark et al.[59] used Monte Carlo simulations on rotational isomeric state chains to investigate the elastomer reinforcement and found that the filler excluded volume effect changes the polymer chain distributions and thus the mechanical properties. Sen and his co-workers[60] employed equilibrium molecular dynamics simulation to study the stress relaxation behavior of polymer nanocomposites, and their results suggested that the mechanical reinforcement could be a consequence of either particle agglomeration or a polymer-based network, depending strongly on the strength and range of particle-polymer interaction, the particle volume fraction, and the state of particle dispersion. By molecular dynamics (MD) simulations, Jaber et al.[35] studied the non-linear behavior of viscosity as a function of shear rate, and they ascribed the non-linear behavior to the formation of "polymer mediated filler network".

Besides, Raos et al.[15, 61] employed a coarse-grained "dissipative particle dynamics" model to perform non-equilibrium MD simulations. They investigated the viscoelastic behavior of filled rubber under oscillatory shear deformations of variable amplitude and frequency and observed the non-linear viscoelastic behavior as a function of shear amplitude. However, their work did not concern on the correlation between the micro-structural evolution and the non-linear behavior.

On the basis of the above description, the mechanism of mechanical reinforcement and non-linear behavior of polymer nanocomposites is still unclear. All previous investigations were focused on either the thermodynamics and kinetics of polymer nanocomposites under quiescent condition through equilibrium simulations and theoretical calculations or the reinforcement mechanism through experimental tools and non-equilibrium simulations. To the best of our knowledge, no simulation work has been performed to characterize the micro-structural evolution during the deformation process and explain the non-linear behaviors of polymer nanocomposites on a microscopic level.

In this study, we employed the coarse-grained model to simulate big systems on large length and time scales, which were composed of 60480 beads in total. Non-equilibrium MD simulations were carried out, including the uniaxial tensile and simple shear tests. By designing different initial dispersion states of NPs before deformation, the stress-strain behaviors were investigated. We then developed a new stress-strain relation to fit the simulated data and derived the modulus-strain relation from the fitted stress-strain curve. Besides, we comprehensively characterized the micro-structural evolutions under deformations. Thus, we analyzed the different underlying mechanisms accounting for the decrease of elastic modulus with the increase of strain in different cases.

2. Model and simulation methods

A coarse-grained model of NPs embedded in a homopolymer matrix was adopted in our simulation. The polymer chains are represented by a bead-spring model, which was developed by Kremer and Grest[62].

The whole system box contains 480 NPs (the volume fraction is 18.55%) and 2000 polymer chains. Each polymer chain contains thirty beads with the diameter equal to σ and the mass equal to m. The NPs were modeled as LJ spheres with the radius R_n equal to 2σ. Since the diameter of a NP is four times that of a polymer bead, the mass is therefore 64 times that of the polymer bead. Note that the radius of gyration of the polymer chains R_g is comparable with the radius of the NPs. Besides, although these chains are rather short compared to real polymer chains, they are already able to display the static and dynamic characteristic behavior of long chains. Each bond in this model corresponds to three to six covalent bonds along the backbone of a real chemical chain when mapping the coarse-grained model to a real polymer.

The truncated and shifted Lenard-Jones (TSLJ) potential is used to compute the non-bonded interactions between polymer beads:

$$U_{ij}(r)=\begin{cases}4\varepsilon_{ij}\left[\left(\frac{\sigma}{r}\right)^{12}-\left(\frac{\sigma}{r}\right)^{6}\right]-U\left(r_{cutoff}\right) & r<2.5\sigma \\ 0 & r\geq 2.5\sigma\end{cases} \quad (1)$$

In this equation, the term $U(r_{cutoff})$, which is a constant, refers to the standard 6-12 LJ potential energy at the cutoff distance. Actually, this term is added here to satisfy the condition that the potential is continuous everywhere. Namely, the interaction is truncated and shifted at the distance r_{cutoff} so that the energy and force are zero. r is the distance between two interaction sites. Note that the LJ interaction is cut off at the distance 2.5σ to include the attractive part, since it is reported in the literature that a negative thermal expansion coefficient would occur without such an attraction. The polymer-polymer interaction parameter is set to ε_{pp}=1.0. Since it is not our aim to study any specific polymers, the mass m and the diameter σ of each bead is set to be unit. Thus all calculated quantities are dimensionless. For example, the number density of polymer beads ρ^* is measured in σ^{-3} units, time is measured in units of $\tau=\sigma(m/k_BT)^{1/2}$, and the units of pressure, stress, and the elastic modulus are all k_BT/σ^3.

The interaction between adjacent bonded polymer beads is represented by a stiff finite extensible nonlinear elastic (FENE) potential:

$$V_{FENE}=-0.5kR_0^2\ln\left[1-\left(\frac{r}{R_0}\right)^2\right] \quad (2)$$

where $k=30\varepsilon/\sigma^2$ and $R_0=1.5\sigma$, guaranteeing a certain stiffness of the bonds while avoiding high-frequency modes and chain crossing.

Moreover, a modified LJ function that offsets the interaction range by R_{EV} is used to model the NP-polymer interaction and NP-NP interaction:

$$U_{ij}(r)=\begin{cases}4\varepsilon_{ij}\left[\left(\frac{\sigma}{r-R_{EV}}\right)^{12}-\left(\frac{\sigma}{r-R_{EV}}\right)^{6}\right]-U\left(r_{cutoff}\right) & r<R_{EV}+r_{cutoff} \\ 0 & r\geq R_{EV}+r_{cutoff}\end{cases} \quad (3)$$

To consider the excluded volume effect of different interaction sites, the interaction range here is offset by R_{EV}. For the NP-polymer interaction and NP-NP interaction, R_{EV} is set to R_n-σ/2 and $2R_n$-σ, respectively. And the actual cutoff is the sum of r_{cutoff} and R_{EV}. The NP-NP interaction parameter and its cutoff distance are set to ε_{nn}=1.0 and $r_{cutoff}=2.5\sigma$, respectively. The NP-polymer interaction parameter ε_{np} and its cutoff distance r_{cutoff} were varied to simulate different interfacial interactions and to obtain different dispersion states of NPs.

The initial configurations are generated that all the polymer chains and NPs are placed in a very large box, so the density of the system is very low. Then the NPT ensemble is adopted to compress the system, where the temperature is fixed at T^*=1.0 by using the Nose-Hoover thermostat and barostat. The purpose of using the NPT ensemble is to control the system volume and thus to keep the reduced number density of polymer beads around ρ^*=0.85, a value corresponding to the density of polymer melts. During the simulation, periodic boundary conditions are imposed in all three dimensions. The velocity-Verlet algorithm is employed to integrate the equations of motion, with a time step $\delta t=0.001\tau$. The obtained structures are further equilibrated under NVT ensemble with T^*=1.0 over a long time so that each chain has moved at least $2R_g$. After enough equilibration, the deformation procedure of the system is then carried out. Although coarse-grained molecular dynamics (CGMD) simulations might not give the correct results beyond equilibrium[63], the method of adopting appropriate equations of motion and periodic boundary conditions can overcome this problem. Actually, the SLLOD equations of motion[64], one of the widely used method for the non-equilibrium case, are implemented in our simulation.

In our simulation, there are two deformation modes. One is the uniaxial tension, which is implemented by changing the box length to $L_0\alpha$ in the z direction, where L_0 is the original box length and α is the tensile elongation. Meanwhile, the box lengths in the x and y directions are reduced to $L_0\alpha^{-1/2}$ simultaneously to maintain a constant box volume. The strain rate is specified as $\dot{\varepsilon}=(L_z(t)-L_z(0))/L_z(0)=0.0327/\tau$, which is the same as that used in the simulation from previous studies[65, 66]. Therefore, the box length $L_z(t)$ as a function of the elapsed time t will change as $L_z(t)=L_z(0)*(1+0.0327*t/\tau)$. By the way, the relaxation time of polymer chains in our simulation is nearly 10τ. Therefore, the strain rate is comparable with the relaxation time of polymer chains, which is consistent with the practical situation during deformation processes of elastomers. It is noted that the obtained qualitative results in our simulation are independent of the strain rate (see Figure 9(b) and Figure S5 in the Supplementary Information). Moreover, the average tensile stress σ_t in the z direction is derived from the deviatoric part of the stress tensor $\sigma_t=(1+\mu)(-P_{zz}+P) \approx 3(-P_{zz}+P)/2$, where $P=\Sigma_i(P_{ii}/3)$ is the hydrostatic pressure.[67] The parameter μ stands for the Poisson's ratio, which is equal to 0.5 in our simulation, because rubbery materials are often regarded as incompressible during the deformation process.

The other deformation mode performed here is the simple shear. For the SLLOD method for shearing system, the Lees-Edwards "sliding brick" boundary conditions[68] are applied. The upper xy plane of the simulation box is shifted along the x direction, so that each point in the simulation box can be thought of as having a "streaming" velocity. This position-dependent streaming velocity

is subtracted from each atom's actual velocity to yield a thermal velocity which is used for temperature computation and thermostatting. The shear strain is defined as $\dot{\gamma}=\delta x/ L_z(0)$, where the offset δx is the transverse displacement distance in the shear direction (x direction for xy deformation) from the unstrained orientation, and $L_z(0)$ is the box length perpendicular to the shear direction. We set the shear strain rate $\dot{\gamma}=0.01/\tau$, which means the shear strain will increase by 0.01 per unit time. The average shear stress σ_s is obtained from the deviatoric part of the stress tensor $\sigma_s=P_{xy}=P_{yx}$.[69]

For the purpose of focusing on the effect of dispersion state of NPs, the deformation process is unified with the same parameter values. Especially, the NP-polymer interaction is set to be moderate attraction (ε_{np}=3.0 and r_{cutoff}=2.5σ). Actually, this setting is reasonable, because during every time step of the deformation process, the relaxation processes of polymer chains cannot finish at the same time. That is, the deformation process is a non-equilibrium dynamic process for the polymer chains, whereupon the disequilibration effect brought out by changing the NP-polymer interaction can be ignored.

During the deformation process, the interactions between the atoms in the basic cell and the image atoms across the cell wall serve to transmit the deformation to the atoms in the basic cell. The strain and the stress used in our simulation are the engineering strain and engineering stress, respectively. More simulation details can be found in our previous studies[70, 71]. All the MD simulation runs were carried out by using the large scale atomic/molecular massively parallel simulator (LAMMPS), which was developed by Sandia National Laboratories.[72]

3. Results and discussions

Since the mechanical properties are intimately related to the initial dispersion state of NPs, we begin our discussion with two typical cases, i.e. aggregation and dispersion of NPs.

3.1 Poor dispersion system

3.1.1 Characterization of NP dispersion

In this simulation system, the poor dispersion state of NPs is obtained by setting the NP-polymer interaction as ε_{np}=0.1. First, we use the snapshot for an intuitive observation of the dispersion state, as shown in Figure 1(a). Clearly, the NPs aggregate to form a three-dimensional network in the polymer matrix. The radial distribution function (RDF) is also calculated to characterize the dispersion state and is presented in Figure 1(b). In this figure, a strong peak appears at approximately r=4σ, indicating direct contact of NPs, which confirms poor dispersion of NPs. Note that the data shown in all figures have been averaged over the simulation time to get statistically significant values.

3.1.2 Stress-strain curve and modulus-strain curve

By performing the uniaxial tensile test, the relationship between the tensile stress σ and the tensile strain ε is obtained, as presented in Figure 2(a). It is worth mentioning that the simulated polymer is in the rubbery state, with the simulated temperature T^*=1.0 above the glass transition temperature of T_g^*=0.49 (see Figure S2 in the Supplementary Information), and the polymer chains are without chemical crosslinking. According to Figure 2(a), the stress grows significantly with the increase of the strain. Note that the linear growths under small deformations (at strains of less than a few percent) and under large deformations (at strains of more than 30%) denote the elastic regimes. In the first elastic regime the growth rate is very high, while in the second elastic regime the growth rate is slow. These simulated results are in good qualitative agreement with the experimental observations. By the way, although CGMD simulations can provide accurate qualitative predictions for the physical properties (mechanical, rheological and so on), quantitative agreement with the experimental data is still unsatisfactory. Therefore, here our simulation work mainly provides a qualitative description of the mechanical behavior of PNCs.

Actually, the instantaneous growth rate, i.e., the slope of the stress-strain curve, at a given tensile strain is the elastic modulus (the tangent modulus of elasticity, $E=d\sigma/d\varepsilon$) at that tensile strain. However, to obtain a smooth modulus-strain curve, we need to first fit the stress-strain curve with an appropriate function and subsequently calculate the derivative.

In Figure 2(a), the traditional Mooney-Rivlin equation

$$\sigma = (a_1 + \frac{a_2}{\lambda})(\lambda - 1/\lambda^2) \quad (4)$$

and several other well-known nonlinear stress-strain relations, such as

$$\sigma = (a_1 + \frac{1.84a_2}{\lambda + 0.84/\sqrt{\lambda}})(\lambda - 1/\lambda^2) \quad (5)^{73}$$

$$\sigma = (a_1 + \frac{a_2}{\lambda - 1/\sqrt{\lambda} + 1})(\lambda - 1/\lambda^2) \quad (6)^{74}$$

$$\sigma = (a_1 + \frac{a_2}{0.72\lambda + 0.61/\sqrt{\lambda} - 0.35})(\lambda - 1/\lambda^2) \quad (7)^{75}$$

are each fitted to the simulated results. In these equations, a_i (i=1,2) are constants and λ=1+ε. Unfortunately, the square of correlation coefficient R^2 is much lower than 1.0 in each case, an indication of poor fit. By the way, although these stress-strain relations generally apply for crosslinked polymer networks, the parameter denoting the contribution of crosslinking is nearly 0, which is consistent with our simulation model here.

In an attempt to better fit the simulated results, we proposed a modified stress-strain equation based purely on mathematical considerations:

$$\sigma = (a_1 + \frac{a_2}{a_3 * \lambda + a_4/\sqrt{\lambda} + a_5})(\lambda - 1/\lambda^2) \quad (8)$$

In this equation, a_i(i=1,2,3,4,5) are the fitting parameters. As shown in Figure 2(a), the modified equation fits the simulation results well with R^2=0.935.

Thus, we take the derivative of the well-fitted stress-strain curve with respect to the tensile strain, and the resulting elastic modulus-strain curve is obtained, as shown in Figure 2(b). The elastic modulus indicates the instantaneous elasticity deformation capacity of materials. The higher the elastic modulus, the less deformable the material. Theoretically, the elastic modulus of an ideal elastomer remains constant during deformations.

3.1.3 Phenomenon similar to "Payne effect"

According to Figure 2(b), starting at a small strain of 0.1%, the elastic modulus of this filled polymer decreases dramatically from 32.31 to about 2.01 at the strain of 10% and reaches a low plateau of 0.15 at strains of larger than 100%. Besides, the initial elastic modulus of this filled polymer is much higher than that of the neat polymer (unfilled), with the initial modulus of the latter being approximately 5.63. Qualitatively, these non-linear characteristics are very similar to the experimentally observed "Payne effect".

It is noted that the elastic modulus of the neat polymer also decreases with increasing strain. Presumably the initial plateau modulus (E_0≈5.63) is attributed to the entropic trapping of polymer chains. However, the simulated initial modulus plateau is shorter than the experimental observation, which may be caused by the short-range interaction between polymer beads. Reasonably, in this work we study the stress-strain curves by using the same force-field and model for all simulated systems. Besides, as a result of the chain slippage effect, the modulus of the neat polymer under large deformation is very low ($E_{\varepsilon\geq 100\%}$≈0.11).

The effect of the chain entanglement on this non-linear behavior should be negligible because the chain length of 30 beads is shorter than the critical entanglement length (N_e≈65±7)[76]. Indeed, when the chain length is increased from 30 beads to 200 beads, the elastic modulus of the neat polymer increases (the initial plateau modulus E_0 increases from 5.63 to 9.15, as shown in Figure S3 in the Supplementary Information). However, in this work we mainly focus on the effect of NPs on the non-linear behavior at constant polymer chain length, and the effect of chain entanglement is not considered.

3.1.4 Underlying mechanism

To further probe the mechanism of this large decrease in elastic modulus with increasing strain, we will analyze the micro-structural evolution during the deformation process.

Two neighboring NPs are considered to form a cluster if their center-to-center distance is smaller than 4.25σ. And in the case of poor dispersion, the NP clusters are linked to form a three-dimensional network structure (the so-called filler network or NP network). Figure 3(a) shows the variation of the number of neighboring NPs with the tensile strain. It is found that the inter-aggregate association is gradually broken up during the deformation process. For instance, the number of neighboring NPs decreases substantially as the strain increases from 0.1% to 10.0%, indicating the dissociation of neighboring NPs. And the abrupt decrease of elastic modulus at small strains is believed to be attributed to the breakup of directly contacting NPs. The snapshots given by Figure 3(b) display the microscopic evolution of the NP network, clearly showing that the NP network ruptures and the large NP clusters become broken up.

Specifically, this three-dimensional NP network structure undergoes four evolution stages.

Although in stage I (at strains below 0.2%) the NP clusters have not begun to break up, as evidenced by the number of neighboring NPs shown in Figure 3(a), the elastic modulus drops quickly. For a better understanding of the underlying mechanism, we calculated the root-mean-squared average force $\langle F_z \rangle$ exerted on each NP in the tensile direction, and the results are shown in Figure 4(a). The instantaneous mobility of NP increases with the increase of the instantaneous force exerted on it. Although $\langle F_z \rangle$ is an average value calculated from NP to NP, however, statistically it reflects the changes of the forces with higher weight. For example, in the stage I, the change of $\langle F_z \rangle$ mainly originates from the extremely large forces on the linking points of the NP. Figure 4(a) shows that the "rigid" NP network endures an enormous force once the system is subjected to tensile loadings, resulting in a very high elastic modulus. On the other hand, this enormous force can induce the dislocation for NPs. Especially, the dislocation of NPs is much more severe at the linking points of the NP network which perform as stress concentration points but are easily deformed, leading to an amplified strain for these linking points over the measured overall strain. As a consequence, these linking points will break up first, namely the rupture of NP network, as illustrated in Figure 4(b).

To confirm the strain amplification effect, we probe the local strain of one typical pair of neighboring NPs at the linking point as a function of stretching time, and the results are shown in Figure 4(c). The local deformation at the linking points exceeds the measured overall strain from the beginning of stretching. Besides, at the overall strain of about 10%, the local strain at the linking points gradually approaches the overall strain, mainly because of the slippage of polymer chains, as will be discussed later.

$\langle F_z \rangle$ reaches a minimum at the strain of approximately 0.2%,, denoting the rupture of NP network. By the way, the decreasing amplitude of $\langle F_z \rangle$ is very large compared with that of elastic modulus, because the resultant force of the NP clusters is actually not so large as the internal atomic force $\langle F_z \rangle$ which pushes the NP clusters relatively compressed, as evidenced by the strain diminution effect inside the NP clusters (Figure 4(c)). In other words, $\langle F_z \rangle$ cannot represent the overall stress or the elastic modulus, but can only reflect the internal instantaneous mobility of NPs.

Moreover, the initial elastic modulus and the tensile strain when the NP network ruptures are intimately related to the strength of the network which is influenced by the NP-NP interaction and NP volume fraction (see sections 3.1.6 & 3.1.7 below). For example, the initial elastic modulus of a pure NP system of close packing could be as large as about 277.09.

In stage II (at strains of 0.2%-0.6%), the number of neighboring NPs still does not change much, but the elastic modulus decreases dramatically. From Figure 4(a), we can see a peculiar increase of $\langle F_z \rangle$. This interesting phenomenon is intrinsically caused by the structural adjustment inside the NP clusters which is brought out by the dislocation accumulation of stressed NP clusters. During this process, the diminished local strain inside the NP clusters is gradually compensated by using the overall strain as benchmark, as shown in Figure 4(c). The structural adjustment of the NP clusters is influenced by the strength of the initial NP network and the size and packing of the NP clusters. If the NP clusters do not form a three-dimensional network, the strain diminution effect on the structural adjustment of NP clusters will be much smaller. And because of the structural adjustment, the NP clusters becomes less compact, resulting in a dramatic decrease of elastic modulus. Meanwhile, the loosening of inter-aggregate association is an important pre-step for the breakup of NP clusters.

In stage III (at strains of 0.6%-10.0%), the NP clusters begin to break up successively in a significant way. To further examine the microscopic deformation of NP clusters, the fraction of NPs with different coordination numbers (CN) normalized by the total number of NPs is calculated and plotted against the tensile strain in Figure 4(d). At strains of 0.6%-10.0%, large NP clusters such as those with CN=7-9 and CN≥10 are severely broken up into smaller ones with the gradual increase of the number of NPs with CN=1-3 and CN=4-6. According to Figure 4(d), the large NP

clusters break up in two steps. As stress concentration points, the linking points of the separated large NPs are first broken up, as indicated by the decrease of the number of NPs with CN=7-9 at strains of 0.6%-3%, and the breakup results in a rapid decrease of elastic modulus. In other words, during this first step, the original NP clusters functioning as "long fibers" are cut to "shorter fibers", so the elastic modulus declines rapidly. And in the second step, the NPs with CN≥10 start to dissociate at strains larger than 3%.

Paradoxically, in stage IV (at strains larger than 10.0%), the profile of the curve in Figure 3(a) at strains from 10% to 327% is similar to the profile of the curve at strains lower than 10%, yet the modulus tends to be steady and is much smaller than the initial modulus (Figure 2(b)). Since the incipient structural break-up of NP clusters leads to a significant drop of modulus, why does the sequential structural breakup under larger deformations (ε>10%) result in a stabilized low modulus? Actually, this phenomenon can be reasonably interpreted by the chain slippage theory, based on the consideration of the two comparable elastic modulus of 0.15 for this filled polymer and 0.11 for neat polymer at large strains. As the strain increases, the polymer chains are oriented and stretched driven by the interaction of NPs and other chains, and accordingly inter-chain sliding occurs. Therefore, the slippage between polymer chains plays a dominant role in the low modulus regime, in spite of the breakup of NP clusters at large strains.

To examine this explanation, we calculated the bond orientation as a function of the strain, and the results are displayed in Figure 4(e). Here we use the second-order Legendre polynomial $\langle P_2 \rangle$ to characterize the bond orientation:

$$\langle P_2 \rangle = \left(3\langle \cos^2\theta \rangle - 1\right)/2 \qquad (9)$$

where θ denotes the angle between a given element (two adjoining monomers in a polymer chain) and the reference direction (the stretching direction). The possible values of $\langle P_2 \rangle$ range from -0.5 to 1.0. Specifically, $\langle P_2 \rangle$=-0.5 indicates a perfect orientation perpendicular to the reference direction, $\langle P_2 \rangle$=0 a random orientation of the segments and $\langle P_2 \rangle$=1.0 a perfect alignment parallel to the reference direction. According to Figure 4(e), there is a distinct orientation of chain segments at strains larger than 10%, reflecting an conformational rearrangement of chains and the resulting slippage of whole polymer chains. This result confirms the above explanation of the low modulus at strains higher than 10%. In addition, the rapid decay of NP-NP interaction (see eq. (3)) with the increase of distance also contributes to the phenomenon.

3.1.5 Evolution of "polymer-mediated filler network"

To further explore the micro-structural evolution, we also calculated the changes of the "polymer-mediated filler network" structures during the deformation, and the results are shown in Figure 5. In the transient "polymer-mediated filler network", fillers are connected to each other through polymer segments. We make the following definitions: the interface beads refer to those polymer beads contacting the surface of one given NP directly, while the connection beads refer to those interface beads connecting two NPs to form a sandwich-like structure. All interface beads and connection beads are constrained by the NPs. Besides, the "loop" structure refers to the molecular sequences of non-interface beads with the two adjoining interface beads located on the same NP. The "bridge" structure is similar to the "loop" structure, but the sequences start and end with interface beads contacting two different NPs. And the "dangle" structure refers to the dangling terminal segments.

According to Figure 5(b), the number of interface beads and connection beads does not change much at strains below 10% (even below 100%) but increases rapidly at strains larger than 100%, signifying the improvement of the interface between the NPs and polymer matrix. However, in consideration of 60000 polymer beads totally, the chain units contacting more than two NPs occupy a very small proportion, implying that the polymer "melt viscosity" cannot be effectively increased. Besides, as the NP clusters break up increasingly, polymer chains have more probability to contact NPs. Actually, these polymer chains interacting with multiple NPs will play an important role under large deformations.

Likewise, the number of different structures such as dangles, loops and bridges changes slightly at small strains and increases significantly at large strains, indicating that many more polymer segments become involved to form the transient "polymer-mediated filler network", according to Figure 5(c).

Meanwhile, the amounts of the three "polymer-mediated filler network" structures are compared. For example, in the initial equilibrium state (unstretched state), the relation generally obeys the equation of $N_{dangles} \approx 2N_{bridges} + 2N_{loops}$, reflecting that one polymer chain can only form either one "bridge" or one "loop" with two dangling terminals. However, as the strain becomes larger, the relation tends to be $N_{dangles} \approx N_{bridges} + N_{loops}$ (ε>300%), indicating that the stretched polymer chain forms two structures ("bridge"+"bridge", "bridge"+"loop" or "loop"+"loop") with two dangling terminals. Additionally, by analyzing the molecular underpinnings of the three structures, we make the hypothetical assumption that the "bridges" and "loops" can provide reinforcement. Therefore, the growth in the number of "bridges" and "loops" per chain should be responsible for the increasing stress under large deformations, proving that polymer chains play an increasing role in the reinforcement of polymer nanocomposites.

3.1.6 Effect of NP-NP interaction and NP-polymer interaction

Now, for the case of the initial poor dispersion of NPs, the effects of the NP-NP interaction strength ε_{nn} and NP-polymer interaction strength ε_{np} on the strain-induced non-linear behavior are investigated, and the results are shown in Figure 6. From Figure 6, we can see higher initial modulus and shorter elastic plateau with the increase of NP-NP interaction, i.e., a more distinct non-linearity of elastic modulus with respect to the strain. This observation confirms again that the breakup of the NP network or clusters formed through direct contact is responsible for the non-linear behavior for the NP aggregation case. Besides, the increase of non-linearity also indicates the enhancement of NP network/clusters with the increase of inter-particle interaction.

Furthermore, Figure 6 also shows the effect of NP-polymer interaction on the non-linear behavior. Obviously, the initial elastic plateau is little affected by the NP-polymer interaction. And a reasonable explanation for the slight increase of the modulus is that stronger NP-polymer interaction reinforces the NPs network.

3.1.7 Effect of NP volume fraction and percolation threshold

Now, we extend our effort to study the effect of NP volume

fraction (φ) on the non-linear behavior. Polymer systems filled with different volume fractions of NPs are established, where the RDFs of NPs each show a sharp peak at approximately r=4σ. The non-linear behavior of these systems are investigated, and the results are shown in Figure 7(a). Clearly, the non-linear behavior becomes more significant with the increase of NP volume fraction, which agrees well with the experiment observations. Besides, according to the inserted VMD snapshots, the NPs with high volume fraction (φ=15.96% and 18.55%) are linked to form three-dimensional network, while the NPs with lower volume fraction (φ=4.53%, 8.67% and 12.47%) are not. Therefore, the elastic modulus of polymers filled with φ=4.53%, 8.67% and 12.47% NPs does not decrease too much at strains below 0.2%. When the initial elastic modulus is plotted against the NP volume fraction in Figure 7(b), the percolation phenomenon can be identified. Specifically, the percolation threshold is approximately 12.5%. Moreover, the non-linearity of the initial elastic modulus with respect to the NP volume fraction increases with the increase of NP-NP interaction strength due to the enhancement of NP network or clusters formed through direct contact.

3.2 Good dispersion system

3.2.1 Characterization of NP dispersion

Now, we shall study the other case where polymer chains are moderately attractive to NPs (ε_{np}=3.0). The snapshot in Figure 8(a) shows that the NPs are spatially isolated in polymer matrix. Besides, according to the RDF in Figure 8(b), we can see that the peak at approximately r=4σ disappears, indicating no direct contact between the NPs. And the peaks located at r=5σ and r=6σ reflect that the NPs are bridged by one or two polymer beads.

3.2.2 Stress-strain curve and modulus-strain curve

Likewise, the stress-strain curve is calculated through the uniaxial tensile test, and the results are shown in Figure 9(a). Following the above steps, we first fit the stress-strain curve by using eq. (8), and then take the derivative of the fitted stress-strain curve to obtain the modulus-strain curve. According to Figure 9(b), the modulus-strain curve corresponding to good dispersion system is similar to that of poor dispersion system, but there are some differences between them. One difference is that the significant decrease of elastic modulus of good dispersion system delays, leading to a more prominent initial plateau. The elastic modulus of good dispersion system changes little at strains below 0.2%. Another obvious difference is that the initial plateau modulus of good dispersion system (E_0≈22.72) is much smaller than that of poor dispersion system. Moreover, the low modulus under larger deformations ($E_{\varepsilon\geq 100\%}$≈0.13) results from the chain slippage effect as well.

3.2.3 Invalidation of the mechanism of the breakup of NP network/clusters

Similarly, we first study the breakup of the NP clusters during the tension process to find out the mechanism of the non-linear behavior of elastic modulus. According to Figure 10(a), no NP clusters form in this good dispersion system, as evidenced by the inexistence of neighboring NPs at strains below 10% strain. And the number of neighboring NPs increases with the increase of strain, indicating a slight aggregation of the NPs. But the maximum NP cluster only contains several NPs, according to Figure 10(b). Since the NPs are dispersed well in polymer matrix, it is impossible to form NP clusters through direct contact, and it can be inferred that there must be some other micro-structural evolutions accounting for the decrease of modulus.

3.2.4 The "rigid" polymer shell layer

Here we propose a polymer shell layer-bridged NP network model that the NPs are connected to each other through "rigid" polymer layers, as shown in Figure 11(a). As we know, in the case of strong NP-polymer interaction, the surrounding polymer chains will be intensely adsorbed onto the surface of NPs, leading to much slower dynamics of polymer chains in the vicinity of the NPs, i.e., the "rigid" polymer layers.

To confirm the polymer shell (interfacial zone) in our simulation system, we investigate the relaxation time (τ_{inf}) and the mean square displacement (MSD) of polymer segments in the vicinity of a given NP under the condition of moderate NP-polymer attraction (ε_{np}=3.0), and the results are presented in Figure 11(b) and 11(c), respectively. To obtain the relaxation time, we need to first calculate incoherent intermediate dynamic structure (IIDS) factor[77-79]:

$$\phi_q^s(t)=\frac{1}{M}\sum_{m=1}^{M}\left\langle \exp\left(\mathbf{iq}\cdot\left[\mathbf{r}_m(t)-\mathbf{r}_m(0)\right]\right)\right\rangle=\frac{1}{M}\sum_{m=1}^{M}\left\langle \frac{\sin(q\Delta r_m(t))}{q\Delta r_m(t)}\right\rangle \quad (10)$$

where M stands for the total number of polymer beads, $[\mathbf{r}_m(t)-\mathbf{r}_m(0)]$ or $\Delta r_m(t)$ means the displacement of scattering center m over a period of time t , and $\boldsymbol{q}$ denotes the momentum transfer describing the spatial scale of the measurement. Then, the obtained IIDS factor curve is fitted by Kohlrausch-Williams-Watts (KWW) function[80, 81]:

$$f(t)=e^{-(t/\tau)^{\beta}} \quad (11)$$

Finally, with the use of the fitted parameters (τ and β), we calculate the relaxation time (τ_{inf}):

$$\tau_{\text{inf}}=\int_0^{\infty}\exp\left[-\left(\frac{t}{\tau}\right)^{\beta}\right]dt=\frac{\tau}{\beta}\Gamma(1/\beta) \quad (12)$$

The dotted extension line in Figure 11(b) is the hypothetical value when the mass center of polymer beads locates at the surface of the NP. Clearly, when the polymer beads approach the NP surface, the relaxation time gradually increases. By the way, the polymer segments contacting the NPs are not totally immobilized. This polymer shell is not in the glassy state, as evidenced by the fact that the relaxation time of polymer beads at the surface of the NPs (τ_{inf}≈0.9) is much smaller than in the glassy state (τ_{inf}≈9.5). Moreover, the polymer beads far away from the NPs (1.5σ from the surface of the NP) recovers its bulk behavior. Thus, the distanced 1.5σ can be defined as the thickness of polymer shell. Besides, the mean square displacement (MSD) shown in Figure 11(c) also exhibits a gradual increase when the polymer beads approach the NPs, and the thickness of the polymer shell is also close to 1.5σ. Therefore, the NPs can be bridged by at most three "rigid" polymer layers. Because of high volume fraction and uniform dispersion of the NPs in this good dispersion system, the NPs are bridged by one or two polymer layers, as proved by the RDF above. It is very reasonable that the connection strength between NPs bridged by one polymer layers is larger than by two layers and three layers. It is noted that the polymer beads in the bridged layer belong to several different chains, thus we name this structure as polymer layer-bridged NP network rather than polymer chain-bridged NP network.

3.2.5 Polymer shell layer-bridged NP network/clusters

On the basis of the above detailed analysis, two NPs can be

considered to form a cluster through the bridging of "rigid" polymer layers, i.e., the broad concept of neighboring NPs. And due to the bridging of polymer layers, the indirect interaction between NPs becomes more soft.

In the good dispersion system, the polymer layer-bridged NP clusters form a three-dimensional network. Similarly, this polymer layer-bridged NP network shows up a high initial elastic modulus and undergoes four evolution stages during the deformation process. However, unlike the NP network through direct contact, this polymer layer-bridged NP network is more stable to sustain its original state when submitted to small deformations, as proved by the smooth decrease of elastic modulus at strains below 0.6%. On the one hand, the uniformly dispersed NPs are submitted to the force evenly. As a result, the material system are not so sensitive to little external perturbation. According to Figure 12(a), the root-mean-squared average force $\langle F_z \rangle$ exerting on each NP in the tensile direction does not change much under small deformations. On the other hand, once the neighboring NPs bridged by polymer layers are forced to generate the relative displacement, the connection beads in the polymer layers will adjust themselves to maintain the bridging between the neighboring NPs. As shown in Figure 12(b), $\langle F_z \rangle$ exerting on the connection beads fluctuates strongly compared with $\langle F_z \rangle$ exerting on the free beads and the interface beads under deformations, indicating the adjustment of connection beads. And because of the adjustment of connection beads, the bridging structures become loose, resulting in the decrease of elastic modulus at strains below 0.6%. Imaginably, the decreasing amplitude of elastic modulus is intimately related to the packing of polymer layer-bridged NPs, the number of polymer layers in the bridging and the NP-polymer interaction (see sections 3.2.7 & 3.2.8 below). By the way, the increase of $\langle F_z \rangle$ on the polymer beads at large strains is attributed to the orientation and slippage of polymer chains.

At stains larger than 0.6%, the polymer layer-bridged NP clusters begin to break up, for the polymer shell layers are no longer able to bridge the NPs, leading to the desorption of connection beads and the weakening of NP-polymer attraction. The total interaction energy of NP-NP and NP-polymer as a function of tensile strain is given in Figure 12(c). The contribution of NP-NP interaction energy to the decrease of elastic modulus is much less than that of NP-polymer interaction energy. Besides, the NP-polymer interaction energy gets higher with the increase of strain, confirming the weakened NP-polymer attraction.

Figure 12(d) shows the number of neighboring NPs bridged by one or two layers as a function of tensile strain. Specifically, the breakup process of polymer layer-bridged NP clusters can also be divided into two steps: the first step is the breakup at strains between 0.6% and 20%, leading to a significant drop of the modulus, and the second step is the continuing breakup at strains larger than 20%, resulting in a stabilized low modulus due to the slippage of polymer chains.

For further confirmation, we also performed the simple shear of the simulation system, and the results are shown in Figure 13(a). The similarity of the two curves of shear modulus and tensile modulus is noticed, i.e., the synchronous change with respect to the strain. The ratio of the tensile modulus E to the shear modulus G obeys the relation $E/G \approx 3.0$, which is consistent with the theoretical prediction for polymeric materials above the glass transition, further validating our non-equilibrium CGMD simulation method. Moreover, the number of neighboring NPs bridged by polymer shell layers at small shear strains is also investigated, as shown in Figure 13(b). Clearly, the breakup process of polymer layer-bridged NP clusters under shear deformations is consistent with that under tensile deformations. Specially, the breakup effect of polymer layer-bridged NP clusters is amplified under shear deformations, revealing that the shear force damages the micro-structures more efficiently than the tensile force.

3.2.6 Evolution of "polymer-mediated filler network"

Now we come back to the issue of the micro-structural evolution under tensile deformations. The variation of the number of the three "polymer-mediated filler network" structures with the tensile strain is shown in Figure 14. In the initial equilibrium state (unstretched state), the numbers roughly obey the relation of $N_{dangles} \approx N_{bridges} + N_{loops}$, indicating that one polymer chain cane form two structures ("bridge"+"bridge", "bridge"+"loop" or "loop"+"loop") with two dangling terminals. However, the number of "bridges" and "loops" decreases at large strains, resulting from the orientation and slippage of polymer chains on the surface of NPs. These long-ranged "bridge" structures and "loop" structures maybe offer a few contributions to the non-linear behavior.

3.2.7 Effect of NP-NP interaction and NP-polymer interaction

Similarly, the effect of NP-NP and NP-polymer interaction on the non-linear behavior is investigated. From Figure 15, we can observe that the non-linearity of elastic modulus with respect to the strain is almost not influenced by the NP-NP interaction. The initial elastic modulus decreases slightly with the increase of NP-NP interaction, presumably because stronger NP-NP interaction makes the polymer layer-bridged NP network less stable.

According to Figure 15, the initial elastic modulus increases with the increase of NP-polymer interaction. In theory, stronger NP-polymer interaction leads to greater restriction of polymer beads surrounding the NPs, resulting in the enhancement of the polymer layer-bridged NP network. By the way, if we map the interaction parameter to the practical experimental system, ε_{np}=10.0 roughly corresponds to the strength of hydrogen bonding.

3.2.8 Effect of NP volume fraction

Now, we focus on the effect of NP volume fraction (φ) on the non-linear behavior. Polymer systems filled with different volume fractions of NPs are established. By setting different values of exclude volume parameter R_{EV} without changing other parameters, the RDF of NPs in each system after equilibration shows peaks at approximately r=5σ and r=6σ, close to that of good dispersion system. Then the uniaxial tensile tests are carried out after changing R_{EV} back, and the results are presented in Figure 16(a). Clearly, the non-linear behavior becomes more prominent with the increase of NP volume fraction, indicating the enhancement of polymer layer-bridged NPs network/clusters. By the way, even though the NP volume fraction is as low as 4.53%, the local network/cluster still forms, as evidenced by the inserted snapshots.

Besides, the initial elastic modulus exhibits good linearity with the increase of NP volume fraction, as shown in Figure 16(b).

However, for stronger polymer layer-bridged NP network/clusters resulted from the stronger NP-polymer interaction strength, the relation between the initial elastic modulus and the NP volume fraction becomes non-linear, which agrees well with the experiment observations[82].

3.2.9 How to effectively reduce the non-linear behavior?

It is well known that this non-linear behavior of elastomer nanocomposites is of great practical importance. For example, the decrease of this non-linearity can reduce the rolling resistance of automobile tires, which is of paramount significance for energy saving and environment protection.

From the above discussions, we know that good dispersion of NPs obtained by improving the compatibility between polymer matrix and the NPs can reduce the non-linear behavior. Therefore, the best strategy to reduce the non-linearity is to disperse the NPs uniformly. For instance, increasing the distances between NPs by force is one good method. According to Figure 17(a), the system filled with 18.44% NPs exhibits a weaker non-linear behavior when the inter-particle distance is larger than 6.0σ. Also for system filled with 4.53% NPs, the non-linear behavior is also reduced with the increase of inter-particle distance. By the way, when the inter-particle distance is larger than 8.0σ, there are no polymer layer-bridged NP clusters forming. It is possible that the long-range "polymer-mediated filler network" structures and the entropic trapping of polymer chains give rise to the decrease of elastic modulus, and therefore the non-linear behavior is very close to that of the neat polymer system. Besides, another effective approach is the surface modification of NPs, such as coating NPs with oligomer or grafting NPs with polymer chains. For example, by using the previous method[70], the system filled with 7.52% grafted NPs was modeled. Each NP is grafted with fifteen polymer chains, and each grafted chain consists of ten beads. The grafted chains are chemically identical with the matrix chains. According to Figure 17(c), the strain-induced non-linearity of elastic modulus is considerable low, demonstrating an effective approach to reduce the "Payne effect".

4. Conclusion

By carrying out non-equilibrium coarse-grained molecular dynamics simulations, we have investigated the changes of elastic modulus as a function of strain for two typical spatial distributions (aggregation vs. dispersion) of NPs in polymer nanocomposites. The relation between the modulus and the strain is derived from the stress-strain curves by performing the uniaxial tension and simple shear. For both the aggregation and dispersion cases, the non-linear behavior, namely the non-linear decrease of the modulus with respect to the strain, is observed. Based on the characterization and analysis of the micro-structural evolution such as the number of neighboring NPs, coordination number(CN) of NPs, root-mean-squared average force exerted on the NPs in the tensile direction, local strain, chain conformations(bridge, dangle, loop, interface bead and connection bead), and the total interaction energy of NP-polymer and NP-NP, it is indicated that the breakup of the NP network or clusters formed through direct contact accounts for the non-linear behavior of the aggregation case. The NP network/clusters undergoes four stages, namely the rupture of the network structure, the structural adjustment and loosening of NP clusters, the breakup of linking points of separated large NP clusters, and the successive breakup of NP clusters on a large scale. The strain amplification effect occurs at the linking points and the strain diminution effect happens inside the NP clusters. For the dispersion case, the elastic modulus is dominated by the NP network formed through the bridging of adsorbed polymer segments among the NPs. The polymer shells surrounding the NPs are composed of polymer beads with low mobility, depending on the distance from the surface of the NPs and the interfacial interaction. However, these adsorbed polymer shells are demonstrated to be far from the glassy state. In addition, for both cases, the elastic modulus reaches a low plateau at large strains due to the orientation and slippage of polymer chains. these interpretations are further validated by tuning the NP-NP interaction, NP-polymer interaction, and the NP volume fraction. Lastly we find that increasing the inter-particle distribution distance and grafting NPs with polymer chains are effective to decrease this non-linearity. In general, our comprehensive simulation results are aimed to uncover the underlying mechanism and provide some guidance on reducing the commonly observed non-linear behavior of polymer nanocomposites.

Acknowledgement

This work is supported by National Basic Research Program of China (973 Program)(2011CB932603), Foundation for Innovative Research Groups of the NSF of China (51221002), Outstanding Young Scientists Foundation of NSF of China (50725310) and National High Technology Research and Development Program of China (863 Program) (2009AA03Z338).

References

1 G. Allegra; G. Raos and M. Vacatello. *Progress in Polymer Science* 2008**, 33**, (7), 683-731.
2 G. Heinrich; M. Kluppel and T. A. Vilgis. *Current Opinion in Solid State and Materials Science* 2002**, 6**, (3), 195-203.
3 J. Jancar; J. F. Douglas; F. W. Starr; S. K. Kumar; P. Cassagnau; A. J. Lesser; S. S. Sternstein and M. J. Buehler. *Polymer* 2010**, 51**, (15), 3321-3343.
4 S. Ahmed and F. R. Jones. *Journal of Materials Science* 1990**, 25**, (12), 4933-4942.
5 J. Liu; L. Zhang; D. Cao; J. Shen and Y. Gao. *Rubber Chemistry and Technology* 2012**, 85**, (3), 450-481.
6 M. Kluppel, The Role of Disorder in Filler Reinforcement of Elastomers on Various Length Scales. In *Filler-Reinforced Elastomers/Sanning Force Microscopy*, Springer Berlin Heidelberg: 2003; Vol. 164, pp 1-86.
7 J. L. Leblanc. *Progress in Polymer Science* 2002**, 27**, (4), 627-687.
8 A. J. Crosby and J.-Y. Lee. *Polymer Reviews* 2007**, 47**, (2), 217-229.
9 L. Zhang; Y. Wu; Y. Wang; Y. Wang; H. Zhang; D. Yu and J. He. *China Synthetic Rubber Industry* 2000**, 23**, (2), 71-77.
10 B. Omnes; S. Thuillier; P. Pilvin; Y. Grohens and S. Gillet. *Composites Part A: Applied Science and Manufacturing* 2008**, 39**, (7), 1141-1149.
11 J. Ramier; C. Gauthier; L. Chazeau; L. Stelandre and L. Guy. *Journal of Polymer Science Part B: Polymer Physics* 2007**, 45**, (3), 286-298.
12 M.-J. Wang. *Rubber Chemistry and Technology* 1998**, 71**, (3), 520-589.
13 S. Bhattacharyya; C. Sinturel; O. Bahloul; M.-L. Saboungi; S. Thomas and J.-P. Salvetat. *Carbon* 2008**, 46**, (7), 1037-1045.
14 Z. Zhu; T. Thompson; S.-Q. Wang; E. D. von Meerwall and A. Halasa. *Macromolecules* 2005**, 38**, (21), 8816-8824.

15 G. Raos; M. Moreno and S. Elli. *Macromolecules* 2006**,** **39**, (19), 6744-6751.
16 Y. Termonia. *Polymer* 2010**,** **51**, (19), 4448-4451.
17 J. Diani; B. Fayolle and P. Gilormini. *European Polymer Journal* 2009**,** **45**, (3), 601-612.
18 J. S. Bergstrom and M. C. Boyce. *Rubber Chemistry and Technology* 1999**,** **72**, (4), 633-656.
19 L. Chazeau; J. D. Brown; L. C. Yanyo and S. S. Sternstein. *Polymer Composites* 2000**,** **21**, (2), 202-222.
20 A. R. Payne. *Journal of Applied Polymer Science* 1965**,** **9**, (6), 2273-2284.
21 L. Mullins and N. R. Tobin. *Journal of Applied Polymer Science* 1965**,** **9**, (9), 2993-3009.
22 G. Huber. *Macromolecules* 2002**,** **35**, (24), 9204-9210.
23 F. Yatsuyanagi; N. Suzuki; M. Ito and H. Kaidou. *Polymer* 2001**,** **42**, (23), 9523-9529.
24 C. Gauthier; E. Reynaud; R. Vassoille and L. Ladouce-Stelandre. *Polymer* 2004**,** **45**, (8), 2761-2771.
25 M. D. Frogley; D. Ravich and H. D. Wagner. *Composites Science and Technology* 2003**,** **63**, (11), 1647-1654.
26 G. Heinrich and M. Kluppel, Recent Advances in the Theory of Filler Networking in Elastomers. In *Filled Elastomers Drug Delivery Systems*, Springer Berlin Heidelberg: 2002; Vol. 160, pp 1-44.
27 M.-J. Wang. *Rubber Chemistry and Technology* 1999**,** **72**, (2), 430-448.
28 P. Cassagnau. *Polymer* 2003**,** **44**, (8), 2455-2462.
29 P. Mele; S. Marceau; D. Brown; Y. de Puydt and N. D. Alberola. *Polymer* 2002**,** **43**, (20), 5577-5586.
30 E. Guth. *Journal of Applied Physics* 1945**,** **16**, (1), 20-25.
31 O. Lame. *Macromolecules* 2010**,** **43**, (13), 5881-5887.
32 J. Frohlich; W. Niedermeier and H. D. Luginsland. *Composites Part A: Applied Science and Manufacturing* 2005**,** **36**, (4), 449-460.
33 K. W. Stockelhuber; A. S. Svistkov; A. G. Pelevin and G. Heinrich. *Macromolecules* 2011**,** **44**, (11), 4366-4381.
34 G. Marckmann; E. Verron; L. Gornet; G. Chagnon; P. Charrier and P. Fort. *Journal of the Mechanics and Physics of Solids* 2002**,** **50**, (9), 2011-2028.
35 E. Jaber; H. Luo; W. Li and D. Gersappe. *Soft Matter* 2011**,** **7**, (8), 3852-3860.
36 V. Pryamitsyn and V. Ganesan. *Macromolecules* 2005**,** **39**, (2), 844-856.
37 M. Surve; V. Pryamitsyn and V. Ganesan. *Langmuir* 2005**,** **22**, (3), 969-981.
38 M. Surve; V. Pryamitsyn and V. Ganesan. *Physical Review Letters* 2006**,** **96**, (17), 177805.
39 M. Surve; V. Pryamitsyn and V. Ganesan. *The Journal of Chemical Physics* 2006**,** **125**, (6), 064903-12.
40 K. Yurekli; R. Krishnamoorti; M. F. Tse; K. O. McElrath; A. H. Tsou and H. C. Wang. *Journal of Polymer Science Part B: Polymer Physics* 2001**,** **39**, (2), 256-275.
41 M. Vacatello. *Macromolecules* 2001**,** **34**, (6), 1946-1952.
42 M. Vacatello. *Macromolecular Theory and Simulations* 2002**,** **11**, (7), 757-765.
43 S. S. Sternstein and A.-J. Zhu. *Macromolecules* 2002**,** **35**, (19), 7262-7273.
44 A.-J. Zhu and S. S. Sternstein. *Composites Science and Technology* 2003**,** **63**, (8), 1113-1126.
45 G. Tsagaropoulos and A. Eisenberg. *Macromolecules* 1995**,** **28**, (18), 6067-6077.
46 A. Papon; H. Montes; M. Hanafi; F. Lequeux; L. Guy and K. Saalwachter. *Physical Review Letters* 2012**,** **108**, (6), 065702.
47 J. Berriot; H. Montes; F. Lequeux; D. Long and P. Sotta. *EPL (Europhysics Letters)* 2003**,** **64**, (1), 50.
48 H. Montes; F. Lequeux and J. Berriot. *Macromolecules* 2003**,** **36**, (21), 8107-8118.
49 J. Berriot; F. Martin; H. Montes; L. Monnerie and P. Sotta. *Polymer* 2003**,** **44**, (5), 1437-1447.
50 H. Montes; T. Chaussee; A. Papon; F. Lequeux and L. Guy. *The European Physical Journal E* 2010**,** **31**, (3), 263-268.
51 S. Merabia; P. Sotta and D. R. Long. *Macromolecules* 2008**,** **41**, (21), 8252-8266.
52 Y. Termonia and P. Smith. *Macromolecules* 1988**,** **21**, (7), 2184-2189.
53 N. Suzuki; M. Ito and F. Yatsuyanagi. *Polymer* 2005**,** **46**, (1), 193-201.
54 R. Perez-Aparicio; A. Vieyres; P.-A. Albouy; O. Sanseau; L. Vanel; D. R. Long and P. Sotta. *Macromolecules* 2013**,** **46**, (22), 8964-8972.
55 T. A. Vilgis. *Polymer* 2005**,** **46**, (12), 4223-4229.
56 N. Jouault; P. Vallat; F. Dalmas; S. Said; J. Jestin and F. Boue. *Macromolecules* 2009**,** **42**, (6), 2031-2040.
57 D. R. Rottach; J. G. Curro; J. Budzien; G. S. Grest; C. Svaneborg and R. Everaers. *Macromolecules* 2007**,** **40**, (1), 131-139.
58 G. D. Smith; D. Bedrov; L. Li and O. Byutner. *The Journal of Chemical Physics* 2002**,** **117**, (20), 9478-9489.
59 J. E. Mark; R. Abou-Hussein; T. Z. Sen and A. Kloczkowski. *Polymer* 2005**,** **46**, (21), 8894–8904.
60 S. Sen; J. D. Thomin; S. K. Kumar and P. Keblinski. *Macromolecules* 2007**,** **40**, (11), 4059-4067.
61 G. Raos and M. Casalegno. *The Journal of Chemical Physics* 2011**,** **134**, (5), 054902.
62 K. Kremer and G. S. Grest. *The Journal of Chemical Physics* 1990**,** **92**, (8), 5057-5086.
63 H. C. Ottinger. *MRS Bulletin* 2007**,** **32**, (11), 936-940.
64 D. J. Evans and G. P. Morriss, Book Statistical Mechanics of Non-equilibrium Liquids. 1990; Vol. Chapter 6.
65 J. Gao and J. H. Weiner. *The Journal of Chemical Physics* 1995**,** **103**, (4), 1614-1620.
66 J. Gao and J. H. Weiner. *Macromolecules* 1996**,** **29**, (18), 6048-6055.
67 D. R. Rottach; J. G. Curro; G. S. Grest and A. P. Thompson. *Macromolecules* 2004**,** **37**, (14), 5468-5473.
68 A. W. Lees and S. F. Edwards. *Journal of Physics C: Solid State Physics* 1972**,** **5**, (15), 1921.
69 D. Long and P. Sotta. *Macromolecules* 2006**,** **39**, (18), 6282-6297.
70 J. Shen; J. Liu; Y. Gao; D. Cao and L. Zhang. *Langmuir* 2011**,** **27**, (24), 15213-15222.
71 J. Liu; Y. Lu; M. Tian; F. Li; J. Shen; Y. Gao and L. Zhang. *Advanced Functional Materials* 2013**,** **23**, (9), 1156-1163.
72 S. Plimpton. *Journal of Computational Physics* 1995**,** **117**, (1), 1-19.
73 G. S. Grest; M. Putz; R. Everaers and K. Kremer. *Journal of Non-Crystalline Solids* 2000**,** **274**, (1-3), 139-146.
74 M. Rubinstein and S. Panyukov. *Macromolecules* 2002**,** **35**, (17), 6670-6686.
75 D. R. Rottach; J. G. Curro; J. Budzien; G. S. Grest; C. Svaneborg and R. Everaers. *Macromolecules* 2006**,** **39**, (16), 5521-5530.
76 J. Qin and S. T. Milner. *Soft Matter* 2011**,** **7**, (22), 10676-10693.
77 B. Christoph; P. Wolfgang; B. Jorg and B. Kurt. *Journal of Physics: Condensed Matter* 1999**,** **11**, (10), 2179.
78 F. W. Starr; T. B. Schroder and S. C. Glotzer. *Phys. Rev. E* 2001**,** **64**, (2), 021802.
79 F. W. Starr; T. B. Schroder and S. C. Glotzer. *Macromolecules* 2002**,** **35**, (11), 4481-4492.
80 B. Kurt; B. Jorg; B. Christoph and P. Wolfgang. *Journal of Physics: Condensed Matter* 1999**,** **11**, (10A), A47.
81 J. Liu; D. Cao and L. Zhang. *The Journal of Chemical Physics* 2009**,** **131**, (3), 034903-10.
82 N. Roy and A. K. Bhowmick. *Polymer* 2010**,** **51**, (22), 5172-5185.

Inserting Graphics

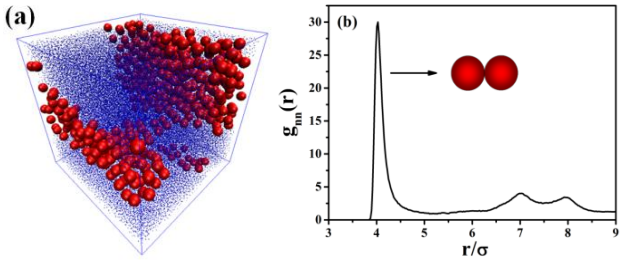

Figure 1. Characterization of the NP dispersion state: (a) The snapshot of the simulated system. Note that the red spheres denote the NPs, and for clarity the polymer chains are represented by blue points.(b) Radial distribution function (RDF) of NPs. The NP-polymer interaction parameter is ε_{np}=0.1.

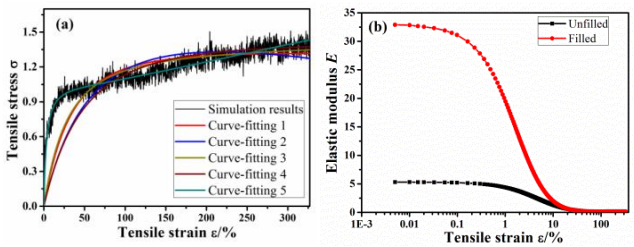

Figure 2. (a) The stress-strain curve calculated in the tensile test and its nonlinear curve-fittings. The fitting equations are $\sigma = (a_1 + a_2/\lambda)(\lambda - 1/\lambda^2)$, $\sigma = (a_1 + 1.84a_2/(\lambda + 0.84/\sqrt{\lambda}))(\lambda - 1/\lambda^2)$, $\sigma = (a_1 + a_2/(\lambda - 1/\sqrt{\lambda} + 1))(\lambda - 1/\lambda^2)$, $\sigma = (a_1 + a_2/(0.72\lambda + 0.61/\sqrt{\lambda} - 0.35))(\lambda - 1/\lambda^2)$, and $\sigma = (a_1 + a_2/(a_3\lambda + a_4/\sqrt{\lambda} + a_5))(\lambda - 1/\lambda^2)$, corresponding to curve-fitting 1, 2, 3, 4 and 5, respectively. All a_i (i=1,2,3,4,5) are fitting parameters, and λ=1+ε. The squares of correlation coefficient (R^2) are 0.361, 0.056, 0.451, 0.106 and 0.935, respectively. (b) The elastic modulus versus the tensile strain for neat polymer and NP filled polymer. Note that the elastic modulus is calculated based on the best curve-fitting 5.

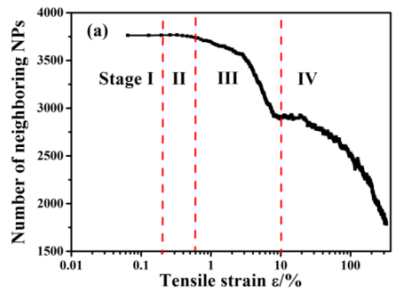

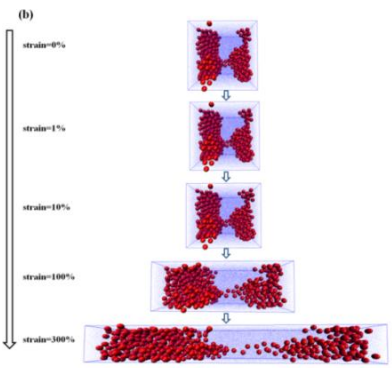

Figure 3. (a) The number of neighboring NPs directly contacting with each other during the deformation process; (b) snapshots of the microscopic deformation of the system along the *z* direction at several typical strains.

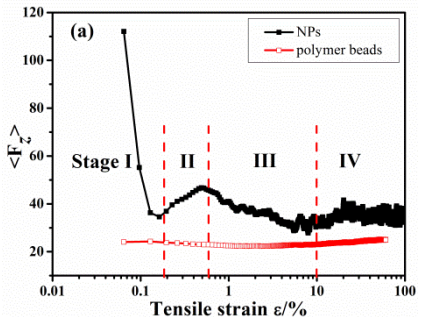

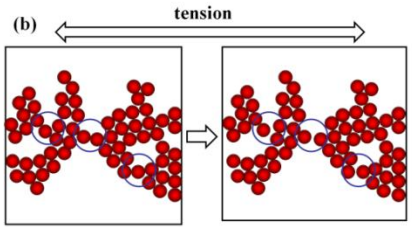

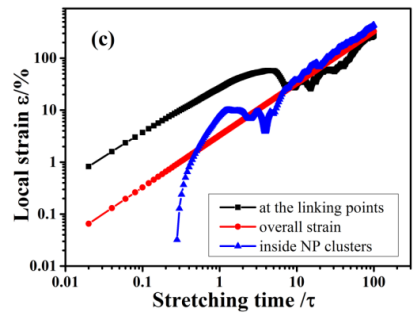

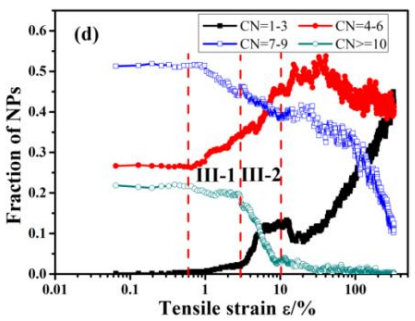

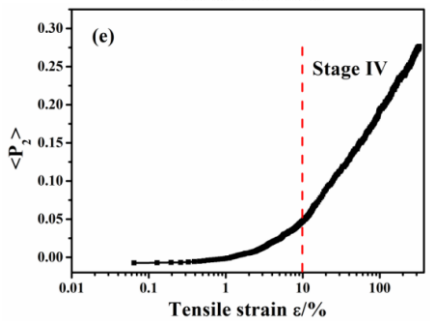

Figure 4. (a) The root-mean-squared average force $\langle F_z \rangle$ exerted on each NP along the tensile direction as a function of the tensile strain; (b) schematic of the evolution of the linking points of the NP network; (c) the local strain at linking points and inside NP clusters, and the measured overall strain as a function of stretching time. Note that the local strain is calculated based on one typical pair of neighboring NPs located at the corresponding position; (d) the fraction of NPs with different coordination numbers (CN); (e) the bond orientation of polymer chains $\langle P_2 \rangle$ during the deformation process.

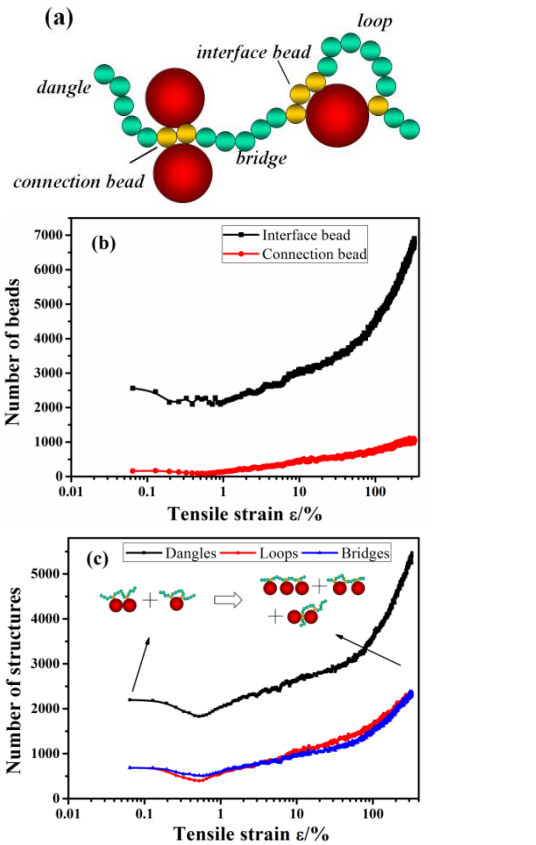

Figure 5. (a) Schematic representation of "polymer-mediated filler network" structures. The red spheres denote the NPs. The green and the yellow spheres represent the polymer beads; (b) the changes of the number of interface beads and the connection beads under deformations; (c) the changes of the number of "dangle" structure, the "loop" structure and the "bridge" structure

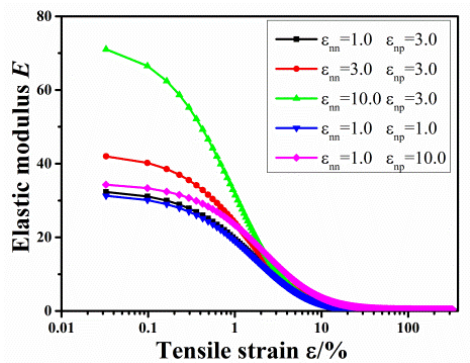

Figure 6. The elastic modulus versus tensile strain for different NP-NP interactions and NP-polymer interactions. The initial states of NPs are all the same with the bad dispersion state above.

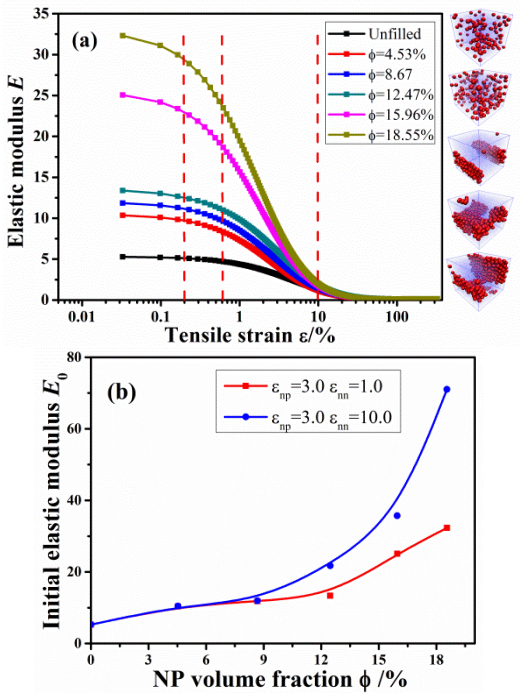

Figure 7. (a) The elastic modulus-strain curves for different NP volume fractions. The RDFs of NPs for all these systems shows a sharp peak at approximately $r=4\sigma$. From top to bottom, the inserted snapshots correspond to the filled systems with the increasing of NP volume fractions; (b) the initial elastic modulus as a function of NP volume fraction.

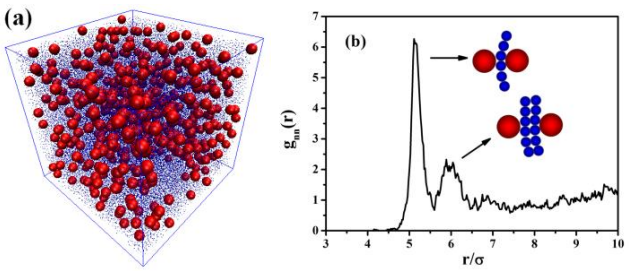

Figure 8. Characterization of the NP dispersion state: (a) The snapshot of the simulated system with good dispersion of NPs. (b) The RDF of NPs. The NP-polymer interaction parameter is ε_{np}=3.0.

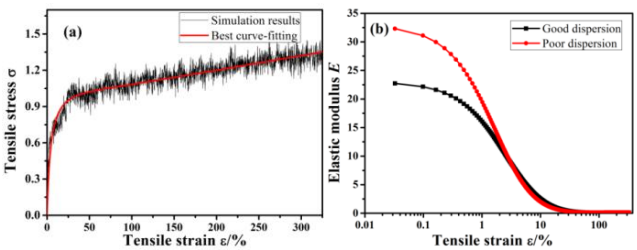

Figure 9. (a) The stress-strain curve obtained from the tensile test and its best non-linear curve-fitting by $\sigma = (a_1 + a_2/(a_3\lambda + a_4/\sqrt{\lambda} + a_5)\lambda - 1/\lambda^2$; (b) The elastic modulus of good dispersion system compared with poor dispersion system.

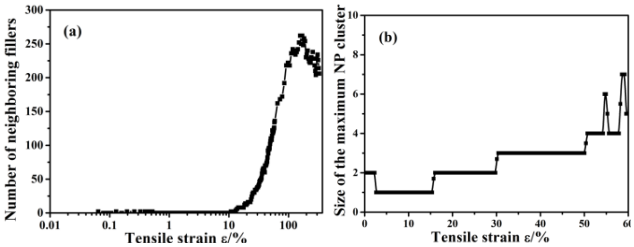

Figure 10.The changes of (a) the number of neighboring NPs directly contacting with each other and (b) the size of the maximum NP cluster during the deformation.

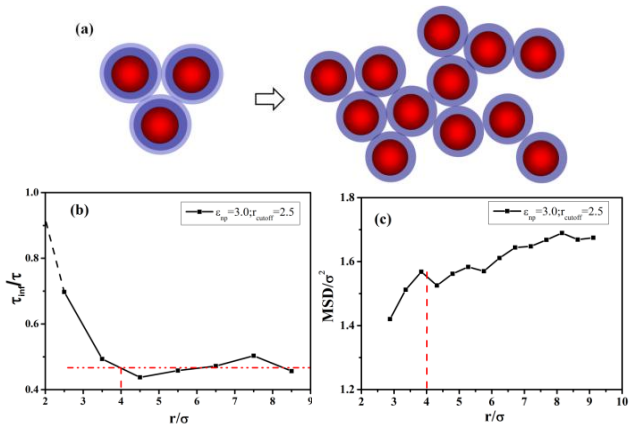

Figure 11. (a) Schematic representation of polymer shell layer model. The red spheres denote the NPs, and the concentric circles with different colors represent polymer layers with different mobility; (b) the relaxation time of polymer segments along the radial distance of the NP. The radius of the NP is 2σ. The interaction between the NP and the polymer beads is set to be moderate attraction (ε_{np}=3.0). The dotted extension line is the hypothetical value when the mass center of polymer beads locates at the surface of the NP, regardless of the occupied volume of the beads; (c) the mean square displacement (MSD) of polymer segments along the radial distance of the NP.

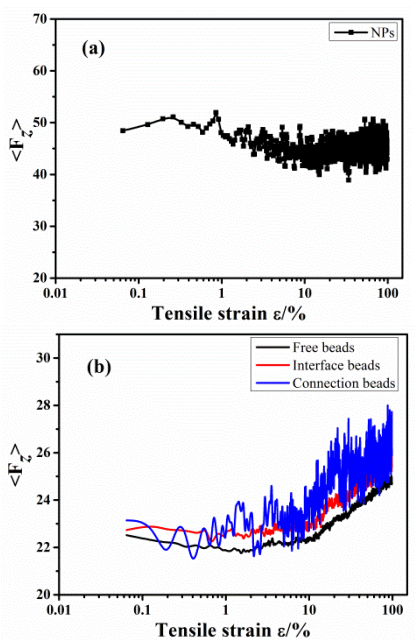

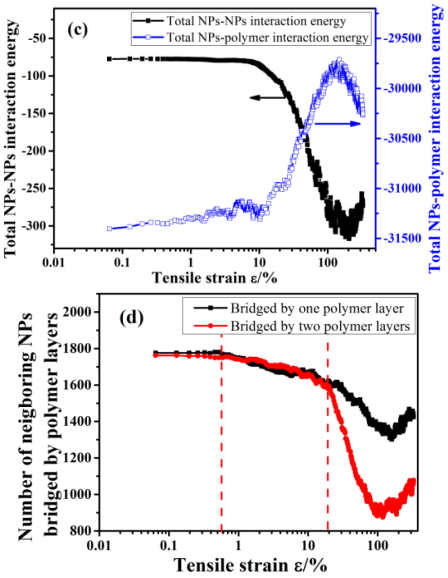

Figure 12. Characterization of polymer layer-bridged NP network: (a) The changes of root-mean-squared average force $\langle F_z \rangle$ exerted on each NP in the tensile direction during the deformation process; (b) The changes of root-mean-squared average force $\langle F_z \rangle$ exerted on polymer beads in the tensile direction; (c) the changes of total NP-NP and NP-polymer interaction energy; (d) the changes of the number of neighboring NPs bridged by polymer shell layers.

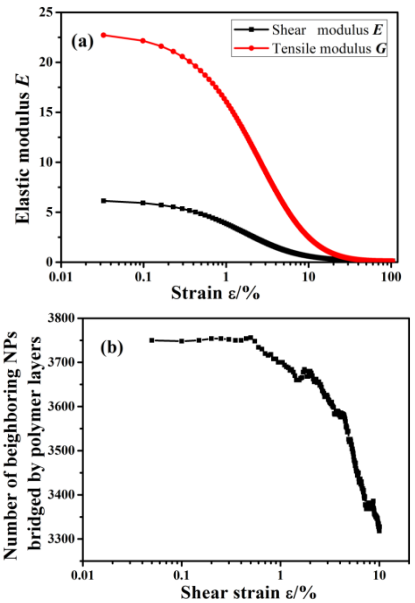

Figure 13. The simple shear: (a) the changes of the elastic modulus derived from the shear test and the tensile test; (b) the change of the number of neighboring NPs bridged by polymer layers at small shear strains.

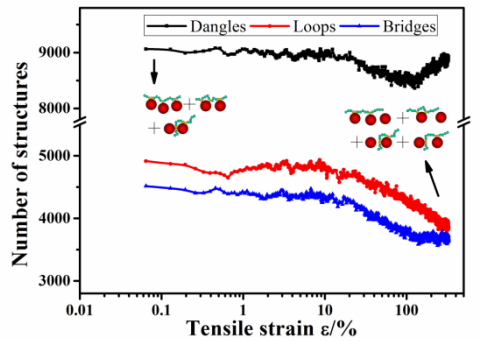

Figure 14. The numbers of "polymer-mediated filler network" structures including the "dangles", "loops" and "bridges" change as a function of the tensile strain

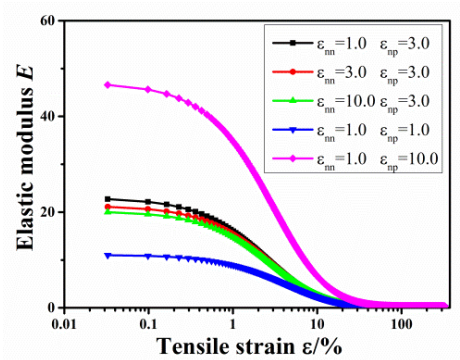

Figure 15. The elastic modulus versus tensile strain for different NP-NP interactions and NP-polymer interactions. The initial state of NPs are all the same with the good dispersion state above.

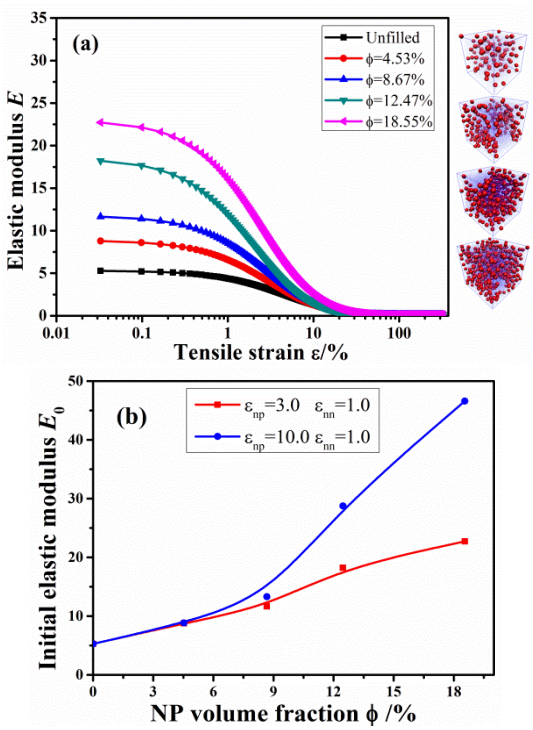

Figure 16. (a) The elastic modulus-strain curves for different NP volume fractions. The RDFs of NPs for all these systems show peaks at approximately $r=5\sigma$ and $r=6\sigma$, close to that of the good dispersion system. From top to bottom, the inserted snapshots correspond to the filled systems with the increasing of NP volume fractions; (b) The initial elastic modulus as a function of the NP volume fraction.

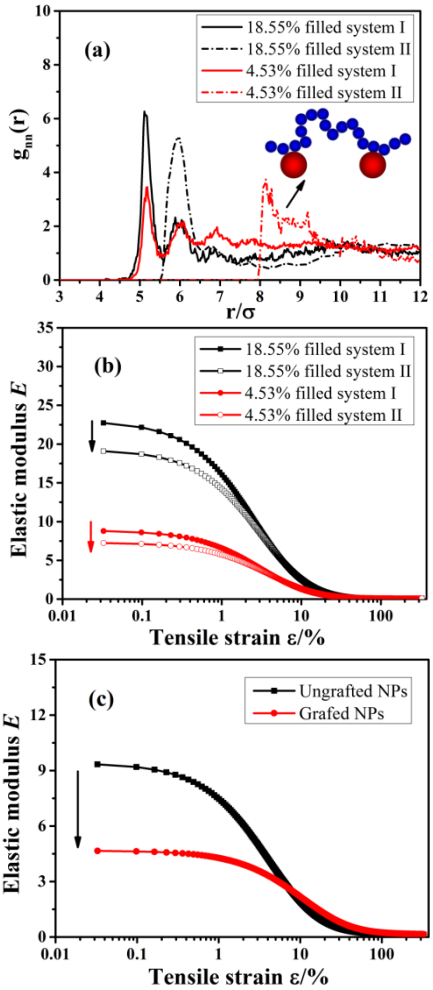

Figure 17. (a) The RDFs of NPs corresponding to different simulation systems; (b) the elastic modulus-strain curves corresponding to different simulation systems; (c) the elastic modulus curves for the ungrafted NPs filled system and the grafted NPs filled system. The NP volume fraction is 7.52% and the interaction between the grafted chains and the matrix chains is set to $\varepsilon_{gm}=1.0$ $r_{cutoff}=2.5$.

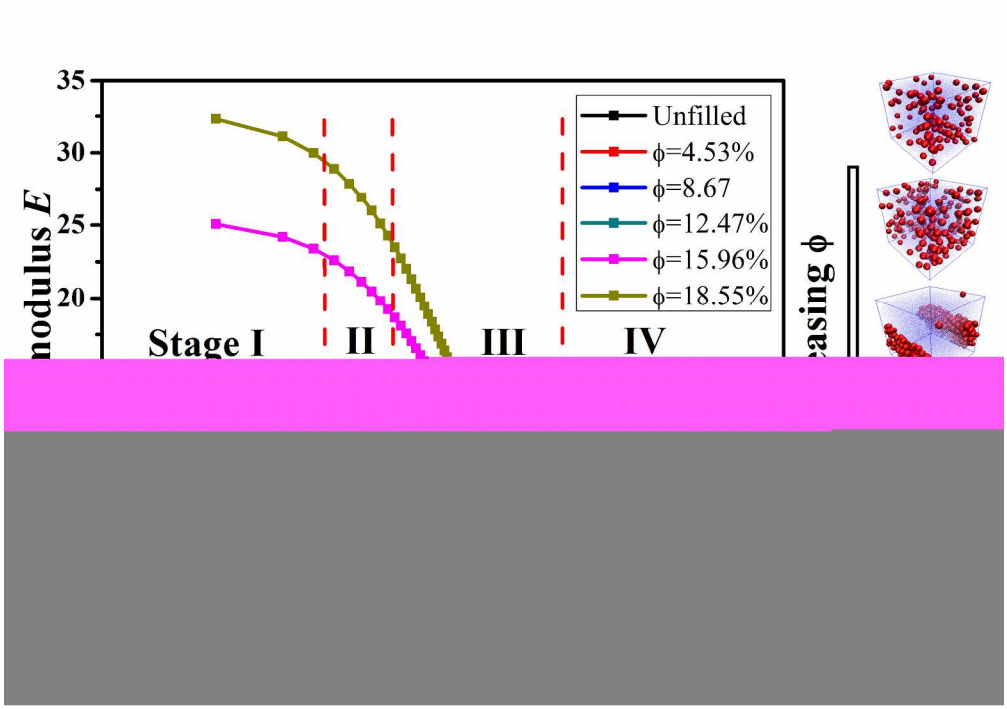

296x209mm (300 x 300 DPI)